

Investigation on intense axial magnetic field shielding with a large melt cast processed Bi-2212 tube

Alaa Dbeyssi^{a,*}, Bertold Froelich^{a,b,1}, Maria Carmen Mora Espi^{a,b}, Frank Maas^{a,b,c}, Luigi Capozza^a, Oliver Noll^a, Yadi Wang^{a,2}, Dexu Lin^{a,3}

^a*Helmholtz Institute Mainz, Staudinger Weg 18, D-55099 Mainz, Germany*

^b*Institute of Nuclear Physics, Johannes Gutenberg University, D-55099 Mainz, Germany*

^c*PRISMA + Cluster of Excellence, Johannes Gutenberg University, D-55099 Mainz, Germany*

Abstract

The feasibility of shielding axial magnetic fields up to 1.4 T, using a Bi-2212 hollow cylinder, is investigated at a temperature of 4.2 K. The residual magnetic flux density along the axis of the tube is measured at external fields of 1 T and 1.4 T. The shielding factor, defined as the ratio between the applied and the residual magnetic flux densities at the center of the tube, is measured to be 32×10^4 at 1 T and 12×10^3 at 1.4 T. The induced current density is evaluated from the measurements taking the thickness of the tube into account. The stability of the measurements over time is also addressed. Numerical simulations for the external and the residual magnetic flux densities are performed and compared to the experimental results. The study shows a high shielding performance of the Bi-2212 superconductor tube at 4.2 K up to 1.4 T.

Keywords: High temperature superconductor, hollow cylinder, magnetic shielding, Bi-2212

1. Introduction

The understanding of the nucleon structure from the QCD theory is one of the central issues in hadron physics. The structure of the nucleon can be described by structure functions that are experimentally accessed through the measurements of electromagnetic processes in scattering and annihilation experiments. In the last decade, the experimental techniques have been substantially and continuously improved yielding new insights in nucleon structure. A recent breakthrough is due to the implementation of polarization techniques and the measurements of spin dependent amplitudes of electromagnetic processes. Among these techniques, polarization experiments that make use of the target polarization have provided important and unique information on the structure of hadrons. Ambitious experimental programs are foreseen at the accelerator facilities using a transversely polarized targets with the aim to achieve a complete and precise description of the hadron structure. In particular, a transversely polarized target at the PANDA experiment [1, 2] is foreseen to measure polarization observables in antiproton-proton

annihilation processes [3]. Changing the spin alignment of the target in spectrometers employing strong magnetic fields such as in PANDA, is a challenging task. In order to operate a transversely polarized target within the PANDA spectrometer, the longitudinal 2 T magnetic field of its solenoid has to be sufficiently shielded. The residual field at an applied external field of 2 T should be as low as possible, to maintain a strong degree of transverse polarization. In addition, a homogenous residual field in a volume that covers the whole region of the target is required. Other important characteristics, needed to avoid spoiling the detection and particle identification efficiency of the spectrometer, are the low material budget introduced by the shielding material and a compact shielding volume of the magnetic field.

Tubular high temperature superconductors are promising solutions to meet the requirements for polarized target experiments [4, 5]. A superconducting tube can be viewed as a concatenation of single rings. A variation of an external magnetic flux in an ideal superconducting ring leads to a near to steady induced current that creates an opposing magnetic field as a consequence of the Faraday law of induction. The set of the rings in a tube is therefore able to induce an opposing magnetic field that follows the distribution of the external one, and to provide a homogeneously distributed residual field in a region sufficiently large for the installation of a polarized target. A superconductor tube of finite thickness is not exactly an ideal conductor, and a penetration of the external magnetic flux above a certain threshold value can be observed. For a

*Corresponding author

Email addresses: adbeyssi@uni-mainz.de (Alaa Dbeyssi), bertoldfroehlich@outlook.de (Bertold Froelich)

¹Currently at: Bundesanstalt für Strassenwesen, Brüderstrasse 53, 51427 Bergisch Gladbach, Germany

²Currently at: North China Electric Power University, Beijing 102206, People's Republic of China

³Currently at: Institute of Modern Physics, Chinese Academy of Sciences, Nanchang Rd. 509, Lanzhou 730000, China

given attenuation level, the induced current density of the shielding material and the thickness of the tube determine the maximum magnetic field that can be shielded. They describe the maximum shielding currents that can flow in the shielding tube.

The shielding performance of the high temperature superconductors such as YBCO, Bi-2212, Pb-doped Bi-2223 and MgB₂, using tubular samples and different manufacturing techniques, has been experimentally tested in different studies [6, 7, 8, 9, 10, 11]. In the present work, the particular choice of Bi-2212 as a high temperature superconducting material is motivated by the measurements of F. Fagnard *et al.* [11]. A large melt cast Bi₂Sr₂CaCu₂O₈ (Bi-2212) hollow cylinder of 80 mm length, 8 mm inner radius and 5 mm wall thickness has been studied in axial magnetic fields at high temperatures above 10 K [11]. At 10 K, a record value of 1 T magnetic field is shielded with a shielding factor of 10^3 [11]. This corresponds to an induced current density of 16 kA/cm². The induced current density in a high-temperature superconductor decreases with rising the temperature. A better performance below 10 K is therefore expected. A Bi-2212 tube is a suitable shielding candidate for polarized target experiments, due to its high transition temperature (92 K), and low density (6.3 g/cm³) and low average-*Z* which minimize the energy loss of the reaction products and less affect their momentum measurement.

In this work, we study the feasibility of shielding intense axial magnetic fields using a high temperature superconducting Bi-2212 tube at a temperature of 4.2 K. A sample of a melt cast Bi₂Sr₂CaCu₂O₈ hollow cylinder from Nexans⁴ with geometrical characteristics in line with the setups of modern high energy physics experiments is used. The dimensions of the tube are listed in Tab. 1. The current density that can be carried by a superconductor material and by consequence its shielding performance depends strongly on the fabrication process. Details on the melt cast process and the centrifugal technique used in the manufacturing of the tube used in this study are discussed in Ref. [12].

The shielding measurements are carried out using a dedicated apparatus consisting of a cryostat filled with liquid helium, two superconducting magnets, and a Hall probe. The setup of the experiment and the results of the measurements are presented in section 2. Numerical simulations are developed and compared to the measurements. They are described in section 3. These investigations help in the development of shielding prototypes that fit the specific requirements of the future polarized target experiments.

2. Experiment

In this section, the experimental measurements for testing the shielding efficiency of the Bi-2212 tube are de-

Length	L_{st}	150 mm
Outer radius	r_{st}	25 mm
Wall thickness	d	3.5 mm

Table 1: The geometrical characteristics of the Bi-2212 shielding tube.

scribed. A longitudinal magnetic field parallel to the wall of the shielding tube is applied, and measurements of the residual field along the axis of the tube are performed at a temperature of 4.2 K. The maximum magnetic field generated at the center is 1.4 T. The longitudinal component of the residual field is measured with a Hall probe placed on the axis of the tube with a manually driven moving system. In addition, stability measurements over several days are taking place at constant external fields. The measurements are carried out in a liquid helium environment. In the first part of the experiment, the external magnetic field is measured without the installation of the shielding tube.

2.1. Setup

The setup of the experiment is illustrated in Fig. 1. A tube system (Fig. 2) consisting of an external magnet, the shielding tube, a Hall probe and an internal magnet (called hereafter a Zero-field magnet) is placed in a dewar filled with liquid helium. An insert is used to hold the tube system and to guide the leads of the dewar. The level of the helium is controlled during the experiment thought the measurements of the dewar weight. A pressure sensor is mounted on the top of the inner part of the dewar. All components used in this experiment are made of non-ferromagnetic materials.

2.1.1. External magnet

The external magnet was designed and constructed to provide intense magnetic fields of at least 2 T. The size parameters of the external magnet are listed in Tab. 2. The wires are made of multi-filamentary Niobium-Titanium (NbTi) with a transition temperature around 9 K. The magnetic field at the center of the external magnet is measured to be 833.6 ± 1.6 G ($1 \text{ G} = 10^{-4} \text{ T}$) at 1 A. The magnet quenches at 24150 ± 90 G. A bipolar high current supply *Kepeco BOP 1000W* is used to operate the external magnet.

Length	L_{em}	138 mm
Radius	r_{em}	31.5 mm
Number of windings per layer	N_{em}	460
Number of layers	n_0	22
Distance between windings	d_w	0.3 mm

Table 2: The geometrical characteristics of the external magnet (*em*).

⁴Nexans SuperConductors GmbH, D-50351 Hürth, Germany

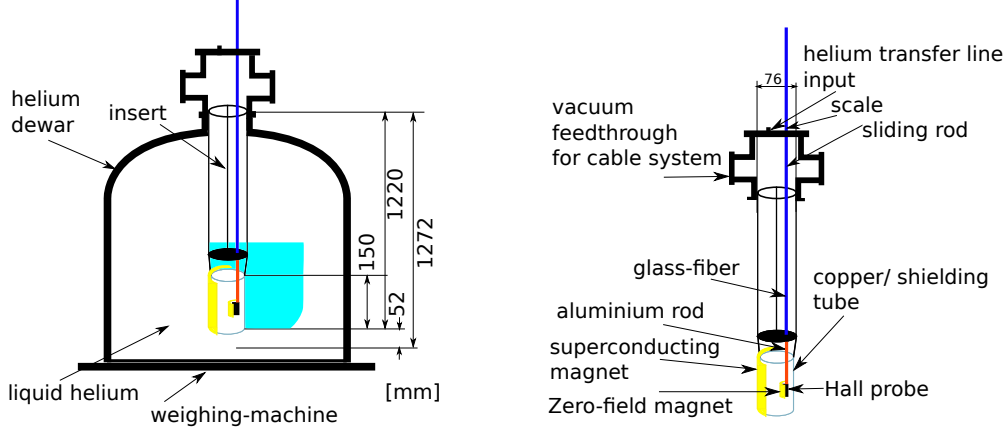


Figure 1: Illustration of the experimental setup: (left) dewar filled with liquid helium to keep the external magnet and the shielding tube at a temperature of 4.2 K, and (right) the insert with the shielding/copper tube and the external magnet. The Hall probe and the Zero-field magnet are mounted on the lower end of a sliding rod (glass fiber rod in the upper section of the insert is connected to an aluminium rod in the lower section). The rod is equipped with a scale to determine the position of the Hall probe. The top of the dewar is equipped with bores that are used to lead the cable system out from inside. The helium transfer line, used to fill the dewar, can be also attached to the system.

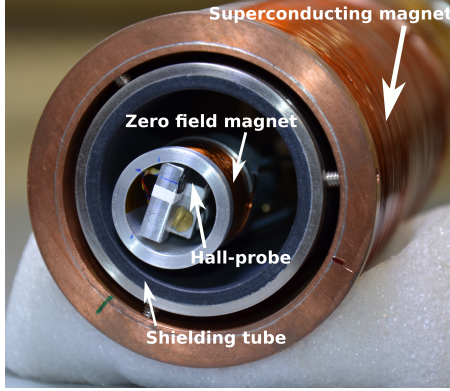


Figure 2: The external superconducting magnet with the shielding tube. The Hall probe is placed on a stick that is moved to its position on the axis of the Bi-2212 tube. In the first part of the experiment, a copper tube is replacing the shielding tube.

2.1.2. Bi-2212 shielding/Copper tube

The shielding tests are performed with the Bi-2212 tube described in Tab 1. It is held by a CuNiMn (LV7) tube with an inner radius of 25 mm and a wall thickness of 2 mm. The tube system is connected to the insert by a copper thread soldered to the tube. In the first part of the experiment, the shielding tube is replaced by a copper tube to measure the external magnetic field.

2.1.3. Hall probe

The longitudinal component of the magnetic fields are measured using a Hall probe from Lake Shore (HGCA 3020). The Hall probe is designed to operate in the temperature range from 1.5 K to 375 K. Corrections to the linear response of the Hall probe, calibrated by Lake Shore, are applied. The accuracy of the Hall probe operated at a nominal Hall probe control current of 100 mA is better than 0.1% up to 2 T. The devices Digistant 64256 T from Burster Präzisionsmesstechnik and Prema 5017 from

Length	20 mm
Inner diameter	22 mm
Number of winding per layer	27
Number of layers	2
Wire diameter	0.75 mm

Table 3: The geometrical characteristics of the Zero-field magnet.

PREMA Semiconductor are used for the control current and the readout of the Hall probe voltage, respectively. The Hall probe holder is fixed on a sliding rod that can be moved along the axis of the shielding tube. The position of the Hall probe is measured using a scale fixed on the top of the dewar.

2.1.4. Zero-field magnet

The Zero-field magnet is a normal conducting coil on an aluminum holder placed directly on the top of the Hall probe to ensure its functionality during the shielding measurements. The geometrical parameters of the Zero-field magnet are given in Tab. 3. The current supply of the Zero-field magnet is provided by the device Instek PSP 603 from GW INSTEK. The maximum field that can be generated by the Zero-field magnet is ~ 210 G. At 1 A, the magnetic field at the center is 21.9 G. The magnetic field strength outside the Zero-field magnet is very small and its induced current in the shielding tube can be neglected.

2.1.5. Data acquisition system

A data acquisition system has been developed to control the power supplies of the magnets and the Hall probe. It also used to read out the Hall probe and the pressure sensor voltages. The readout and the control devices are connected to a computer running the EPICS software via a RS-232 interface. The time interval between the read-out cycles is 2 seconds. The data are synchronized with a

time delay of less than one second, and they are written in the same output stream.

2.2. Description of the measurements

Using the setup described above, the following measurements are carried out :

- measurements of the the external magnetic flux density B_{ext} without the Bi-2212 shielding tube: the response of the generated magnetic field to the applied current I_{ext} is measured at the center of the external magnet. In addition, B_{ext} is measured along the axis of the external magnet at fixed I_{ext} .
- measurements of the residual magnetic flux density B_{res} at the center of the Bi-2212 shielding tube by increasing and decreasing B_{ext} in the intervals $[-1, 1]$ T and $[-1.4, 1.4]$ T.
- measurements of B_{res} along the axis of the tube at fixed B_{ext} (1 T and 1.4 T).
- measurements of B_{res} with the Zero-field magnet: in the presence of the shielding tube, a very low signal is expected to be detected by the Hall probe. The known magnetic field generated by the Zero-field magnet placed between the Hall probe and the shielding tube is used to test the response of the Hall probe. The current of the Zero-field magnet is increased gradually up to 1 A. B_{res} is determined from the linear fit to the measured magnetic flux density as a function of the increased current. In the following, this value is called "inc." value. Another value, called "dec.", is obtained in the same way by decreasing the current of the Zero-field magnet. Before the start of the "inc." and "dec." measurements, the Zero-field magnet is turned off and two additional data points, called "0 inc." and "0 dec." are collected, respectively.
- stability measurements over days of B_{res} at the center of the Bi-2212 tube, at fixed values of B_{ext} (1 T and 1.4 T).

In each measurement series of B_{res} , an offset defined as the measured B_{res} without applying any magnetic field, is determined experimentally and subtracted from the data.

2.3. Analysis of the measurements

2.3.1. Estimation of the uncertainty on the measurement of the residual magnetic field

The uncertainty in the measurement of B_{res} is mainly given by the uncertainty on the readout of the Hall probe voltage. The fluctuations of the Hall probe voltage are studied by recording the output of the *Prema 5017* voltmeter for about 12 hours. The output is divided into six data sets corresponding each to two hours of data taking. Each data set is fitted with a Gaussian function where its standard deviation σ is determined. The largest value

$\sigma = 0.14 \mu\text{V}$ is taken as the statistical error of the measurements. At the helium temperature, this value corresponds to a statistical error of 0.17 G on the measurement of B_{res} . In addition, the drift given by the manufacturer for a 24 h measurement is less than $0.6 \mu\text{V}$ (0.73 G). The two uncertainties are summed in quadrature and a conservative estimate for the uncertainty on one single measurement of B_{res} , 0.75 G, is considered in this analysis.

2.3.2. Measurement of the external magnetic flux density

A stable power supply current for the external magnet is obtained by operating the *Kepco BOP 1000W* in a voltage mode. The B_{ext} is measured as the mean value of the data points collected with a stable current for at least 20 seconds. The same procedure is applied for the measurement of B_{res} . The measured values of B_{ext} as a function of I_{ext} are shown in Fig. 3. The data are well described by a second order polynomial function

$$\begin{aligned} B_{ext} &= aI_{ext} + bI_{ext}^2 + c, \\ a &= 833.03 \pm 1.17 \text{ [G/A]}, \\ b &= 0.58 \pm 0.14 \text{ [G/A}^2\text{]}, \\ c &= 9.42 \pm 1.65 \text{ [G]} \end{aligned} \quad (1)$$

where the parameters a , b and c are determined from the fit to the data shown in Fig. 3. The uncertainty of the data is mainly determined by the error in the setting of I_{ext} which is propagated to the uncertainty on B_{ext} . The

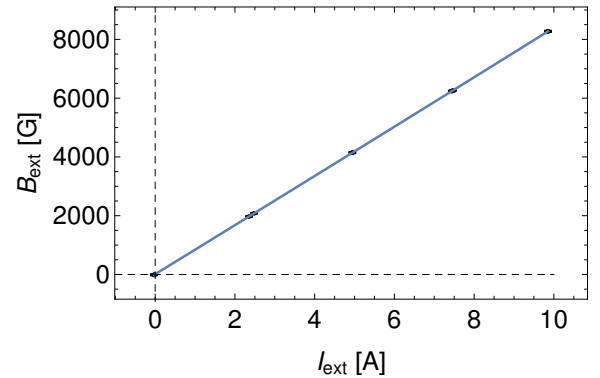


Figure 3: The measured values of B_{ext} as a function of I_{ext} (1 G= 10^{-4} T). The blue solid curve shows the fit to the data based on Eq. 1. The χ^2/ndf of the fit is 0.2.

measurements of B_{ext} along the axis of the magnet are shown in Fig 4. During these measurements, the maximum variation of I_{ext} is within 0.1%. The mean value is determined to be $I_{ext} = (9.88 \pm 0.01)$ A, and the measured value of B_{ext} at the center of the magnet is (8280 ± 10) G.

2.3.3. Measurements of the residual magnetic flux density at 1 T

The Bi-2212 is installed at the center of the external magnet and B_{res} is measured by the Hall probe while varying B_{ext} between ~ -1 T and $\sim +1$ T. The values of B_{res}

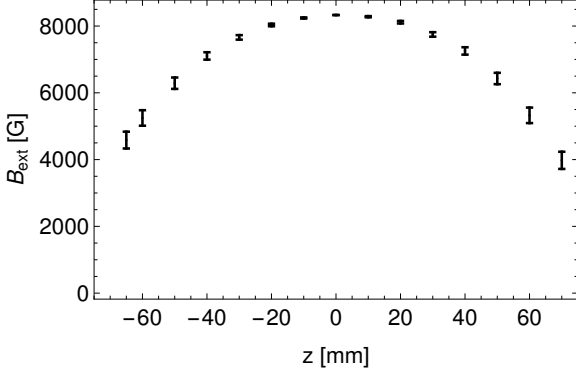


Figure 4: The measured values of B_{ext} ($1 \text{ G}=10^{-4} \text{ T}$) along the axis of the external magnet at $I_{ext} = (9.88 \pm 0.01) \text{ A}$.

Mode	$B_{res} [\text{G}]$	$B_{ext} [\text{G}]$	χ^2/ndf
inc.	0.2 ± 0.13	-17 ± 2	0.1
dec.	0.03 ± 0.12	-17 ± 2	0.6
inc.	0.3 ± 0.13	10140 ± 14	0.5
dec.	0.31 ± 0.12	10130 ± 14	0.5

Table 4: The values of B_{res} ($1 \text{ G}=10^{-4} \text{ T}$), after the the offset subtraction, determined from the linear fits to the data collected with the Zero-field magnet (Fig. 7).

measured at the center of the Bi-2212 shielding tube are shown in Fig. 5. No increase of B_{res} is observed. The mean value of the B_{res} measurements, $\mu_{meas} = -1 \text{ G}$, is defined as the offset of these measurements. Figure 6 shows the distribution of B_{res} after the offset subtraction. The statistical mean and fluctuation of this distribution are found to be $\mu_{res} = B_{res} = 0 \text{ G}$ and $\sigma_{res} = \Delta B_{res} = 0.016 \text{ G}$, respectively. In the calculation of the μ_{meas} and σ_{res} values, the data from the operation of the Zero-field magnet are also included. The linear fits to these data points, collected at $B_{ext}=17 \text{ G}$ (stable measurements with zero external current are not feasible with the used power supply device) and 10140 G , are shown in Fig. 7. The results of the fits on the determination of B_{res} , after the subtraction of the offset -1 G , are summarized in Tab. 4. It is shown that no residual field is entering the shielding tube by increasing B_{ext} up to 1 T .

The current density J_{ind} of the Bi-2212 tube and its uncertainty are calculated as

$$J_{ind} = \frac{B_{ext}}{\mu_0 d},$$

$$\sigma_J^2 = \frac{\sigma_{ext}^2}{(\mu_0 d)^2} + \frac{B_{ext}^2}{(\mu_0 d^2)^2} \sigma_d^2 \quad (2)$$

where $B_{ext} = (10140 \pm 14) \text{ G}$ is the shielded external field, $d = 3.5 \pm 0.2 \text{ mm}$ is the wall thickness of the tube, and $\mu_0 = 4\pi \cdot 10^{-7} \text{ (Vs/A m)}$. The main source of uncertainty in the determination of $J_{ind} = (23 \pm 2) \times 10^3 \text{ (A/cm}^2\text{)}$ comes from the uncertainty on the measurement of the wall thickness σ_d of the tube. The shielding factor SF is

	0 to 10 h	20 h to 100 h
$B_{ext} [\text{G}]$	10081 ± 14	$(100 \pm 2) \times 10^3$
$B_{res} [\text{G}]$	0.000 ± 0.008	0.499 ± 0.003

Table 5: The mean values of B_{res} (after the offset $(-0.751 \pm 0.008) \text{ G}$ subtraction) and B_{ext} ($1 \text{ G}=10^{-4} \text{ T}$) from the stability measurements (Fig. 8).

defined as

$$SF = \frac{B_{ext}}{B_{res}}. \quad (3)$$

In the present case ($B_{res} = 0$), the SF is calculated using a MC simulation method. A normal distribution for B_{ext} (B_{res}) is generated with a mean and a variance fixed respectively by the measured value $B_{ext} = (10140 \pm 14) \text{ G}$ ($B_{res} = 0 \pm 0.016 \text{ G}$). The two distributions for B_{ext} and B_{res} are used to calculate a probability density function for the estimation of the shielding factor. At a confidence level of 95%, the shielding factor is determined to be $SF_{2\sigma} = 3.2 \cdot 10^5$.

The stability of the residual field was measured at a constant external magnetic field of 1 T for about four days. The data are shown in Fig. 8. An increase step of the residual field is observed after ~ 9 hours followed by a stable behavior. The mean values of the measured B_{res} and B_{ext} are summarized in Tab. 5.

The residual field along the axis of the shielding tube is measured at an external field at the center of the tube equal to $(10330 \pm 14) \text{ G}$. The results of the measurements are shown in Fig. 9. A shielded length, where B_{res} is lower than 1 G , of 80 mm is observed from a total length of 150 mm .

2.3.4. Measurements of the residual field at 1.4 T

In this part of the experiment, B_{ext} is varying between -1.4 T and 1.4 T and B_{res} is measured at the center of the Bi-2212 tube, as shown in Fig. 10. The data include also the measurements performed using the Zero-field magnet as described in the previous section. The results of these measurements are listed in Tab. 6. A slight increase of the B_{res} values, compared to the measurements performed at 1 T , is observed.

The residual field is calculated as follows

$$B_{res} = B_{res}^{max} - B_{res}^0, \quad (4)$$

where B_{res}^{max} and B_{res}^0 are the values of the residual field at $B_{ext} = (14640 \pm 30) \text{ G}$ and $B_{ext} = (17 \pm 2) \text{ G}$, respectively. The residual fields B_{res}^{max} and B_{res}^0 are determined from the average over the Zero-field magnet measurements. The results are given in Tab. 6.

The shielding factor and the current density at 1.4 T are determined to be $SF = \frac{B_{ext}}{B_{res}} = 122 \times 10^2$ and $J_{ind} = (33 \pm 3) \times 10^3 \text{ A/cm}^2$ (Tab. 7), respectively.

The stability of the residual field of the shielding tube at a constant external magnetic field of $(14765 \pm 30) \text{ G}$ is measured for 14 hours (Fig. 11). The value of B_{res} is

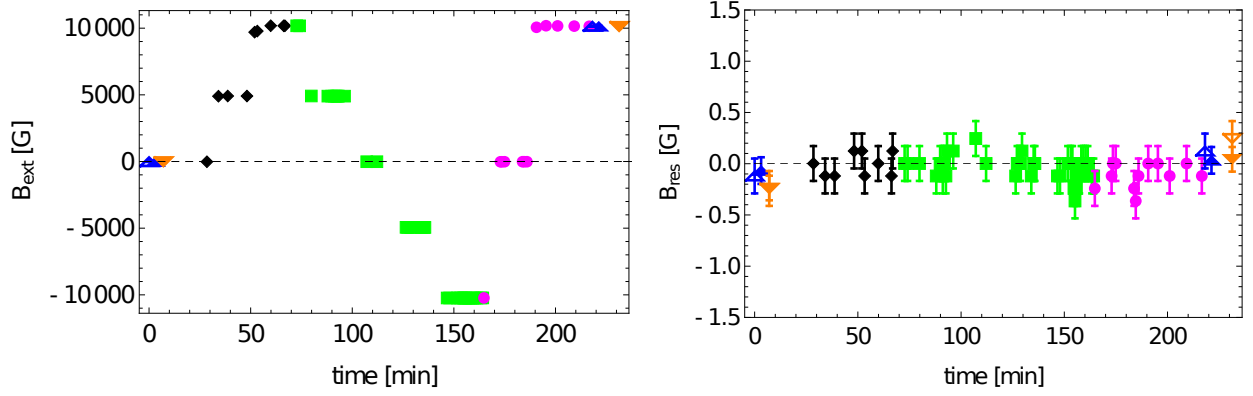


Figure 5: The values of (left) B_{ext} and (right) B_{res} ($1 \text{ G}=10^{-4} \text{ T}$) measured as a function of the time: B_{ext} is 1) increased up to 1 T (black points); 2) decreased down to -1 T (green squares); and 3) increased again up to 1 T (magenta points). The values of B_{ext} are determined from Eq. 1. The data obtained from the operation of the Zero-field magnet are shown with blue filled triangles (inc. value), orange filled triangles (dec. value), blue open triangles (0 inc. value), and orange open triangles (0 dec. value).

time [min]	B_{res} [G]	B_{ext} [G]	χ^2/ndf
0 (inc)	-0.22 ± 0.13	17 ± 2	0.2
6 (dec)	-0.43 ± 0.12	17 ± 2	0.9
10 (inc)	-0.19 ± 0.13	17 ± 2	0.2
14 (dec)	-0.4 ± 0.12	17 ± 2	1.1
67 (inc)	0.72 ± 0.13	14640 ± 30	0.4
72 (dec)	0.86 ± 0.12	14640 ± 30	0.3
77 (inc)	1.04 ± 0.13	14630 ± 30	1.3
83 (dec)	0.98 ± 0.12	14630 ± 30	0.4

Table 6: The values of B_{res} ($1 \text{ G}=10^{-4} \text{ T}$), after the the offset (-1.44 ± 0.04) G subtraction, determined from the linear fits to the data collected with the Zero-field magnet at $B_{ext}=17 \text{ G}$ and 14640 G . The measurements show a penetration of the external field into the shielding tube 1.4 T .

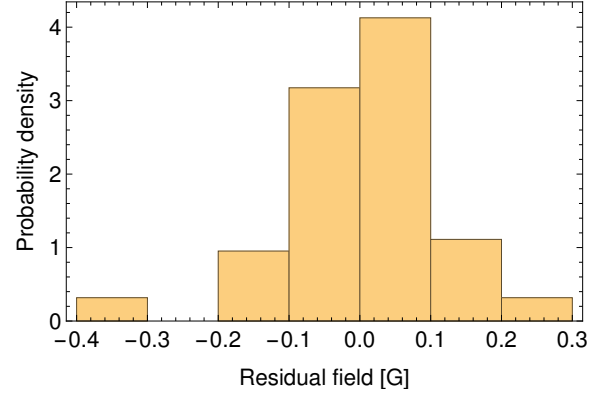


Figure 6: The values of B_{res} ($1 \text{ G}=10^{-4} \text{ T}$) after the offset subtraction ($\mu_{meas}=-1 \text{ G}$), while increasing and decreasing the B_{ext} to 1 T and -1 T, respectively.

increased up to $2.7 \pm 0.15 \text{ G}$ after 14 hours. The residual field along the axis of the tube is measured at constant $B_{ext} = 14793 \pm 30 \text{ G}$. The shielded length, with a residual field less than 2 G, is 80 mm from a total length of 150 mm. The data are shown in Fig. 12.

3. Numerical simulations for shielding of a magnetic field with a Bi-2212 tube

In addition to the experimental investigations on the shielding of external magnetic fields with a Bi-2212 tube, numerical simulations are performed and compared to the measurements. The simulations will be used as a tool to design a prototype of geometrical characteristics that fits the requirements of a polarized target experiment with the PANDA spectrometer.

The induced current in a shielding tube which creates the shielding magnetic counter-field, depends on the position along the axis of the tube. A simple Biot-Savart calculation with the assumption of a homogeneous current in the whole tube is not sufficient to calculate the residual

B_{ext} [G]	14640 ± 30
B_{res} [G]	1.22 ± 0.06
SF	$(12 \pm 1) \times 10^3$
J_{ind} [A/cm ²]	$(33 \pm 3) \times 10^3$

Table 7: The values of B_{ext} , B_{res} ($1 \text{ G}=10^{-4} \text{ T}$), SF and J_{ind} measured at the center of the Bi-2212 tube. The offset (-1.44 ± 0.04) is subtracted from the data.

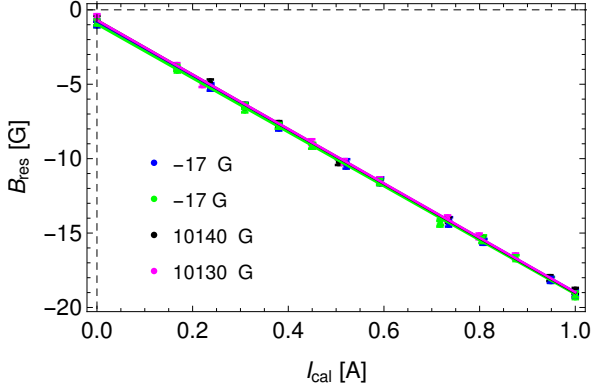


Figure 7: The measured values of B_{res} ($1 \text{ G}=10^{-4} \text{ T}$) as a function of I_{cal} at constant values of B_{ext} (17 G and 10140 G): I_{cal} is increased (blue and black points) and decreased (green and magenta points). The solid lines represent the linear fits to the data points.

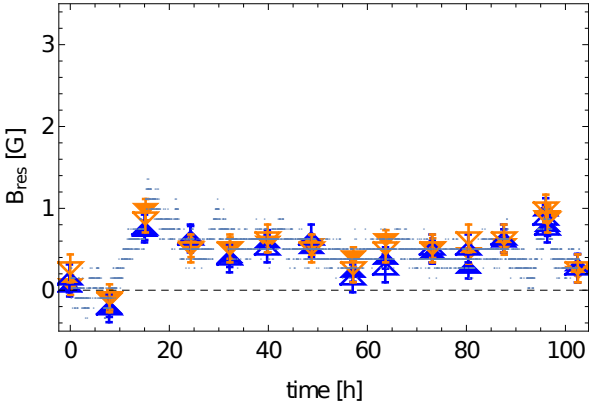


Figure 8: Stability measurements of the residual field using the Bi-2212 shielding tube at $B_{res} \sim 1 \text{ T}$. The total time of the measurements is four days. The data obtained from the operation of the Zero-field magnet are shown with blue filled triangles (inc. value), orange filled triangles (dec. value), blue open triangles (0 inc. value) and orange open triangles (0 dec. value)

magnetic field. Therefore, the induced current is calculated by using the exact forms of the Maxwell equations in integral form and the Biot-Savart law. The method is based on the discretization of the shielding tube into rings [13] as shown in Fig. 13. The tube is divided in $N_{st} = 3750$ equidistant rings and the distance between the rings is $d_R = 0.04 \text{ mm}$. The assumption of ideal circular conducting rings is used. Based on Faraday's law, the magnetic flux through the surface bounded by an ideal conductor is constant. Assuming a zero residual magnetic flux (F^{res}) in the shielding tube at the beginning of the process, the external magnetic flux (F^{ext}) is fully compensated by the induced flux (F^{ind}) inside the shielding tube ($F^{ind} = -F^{ext}$). This property is used in the calculation of the induced current and the induced magnetic flux density of the shielding tube. F^{ext} is calculated using the parameters of the external magnet. The simulations can be applied to any size of the shielding tube or the external magnet. In the following, the geometrical parameters

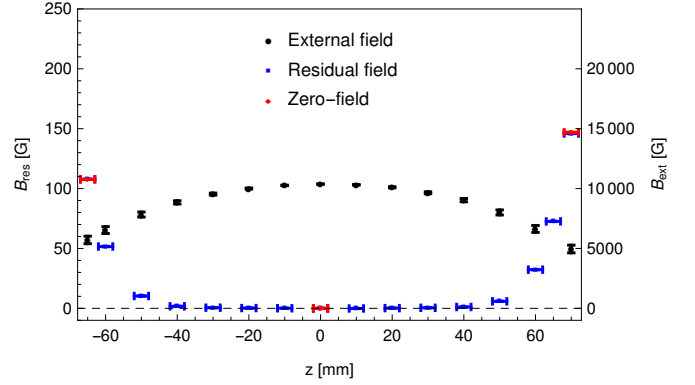


Figure 9: The distribution of B_{res} ($1 \text{ G}=10^{-4} \text{ T}$) measured along the axis of the Bi-2212 tube (blue squares). The black points show the distribution of B_{ext} ($\sim 1 \text{ T}$ at the center). The red diamonds are the values of B_{res} determined from the operation of the Zero-field magnet.

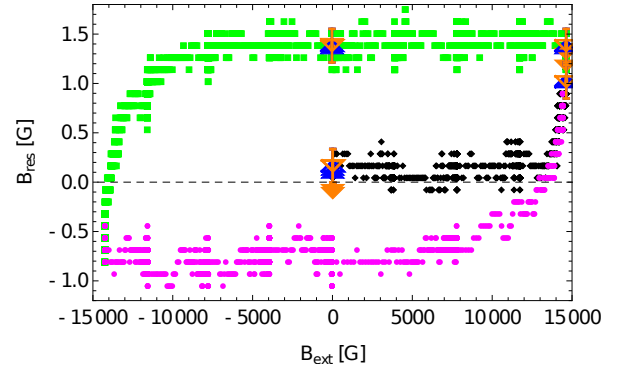


Figure 10: The measured values of B_{res} as a function of B_{exp} ($1 \text{ G}=10^{-4} \text{ T}$): B_{ext} is 1) increased up to 1.4 T (black points); 2) decreased down to -1.4 T (green squares); 3) and increased again up to 1.4 T (magenta points). The values of B_{ext} are calculated using Eq. 1. The data obtained from the operation of the Zero-field magnet are shown with blue filled triangles (inc. value), orange filled triangles (dec. value), blue open triangles (0 inc. value) and orange open triangles (0 dec. value)

for the tube and the magnet used in the experiment, are considered.

3.1. Calculation of the external magnetic flux density

The external magnet used in the experiment has 460 windings and 22 layers ($n_0 = 22$). An example for the layout cross section of 2 windings and 3 layers is shown in Fig. 14. A winding of the external magnet has a simple geometry of a circular closed loop in approximation to a helix of a small height of one wire diameter compared to the total length of the external magnet. A reference system where the winding of the external magnet is located at the center of the x-y plane, and creates a magnetic flux density in the x-z plane, is considered. The z component of the magnetic flux density at a position $P(r_x, r_z)$ in the x-z plane is calculated via the Biot-Savart law [14] as

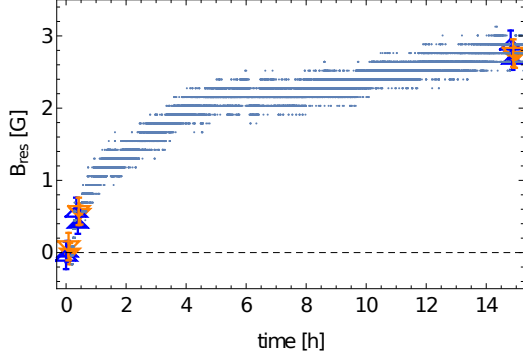


Figure 11: The measured values of B_{res} ($1 \text{ G} = 10^{-4} \text{ T}$) at the center of the shielding tube at a constant B_{ext} of $\sim 1.4 \text{ T}$. The total time of the measurements is ~ 14 hours. Symbols are as in Fig. 8. The offset (1.14 ± 0.08) G is subtracted from the data.

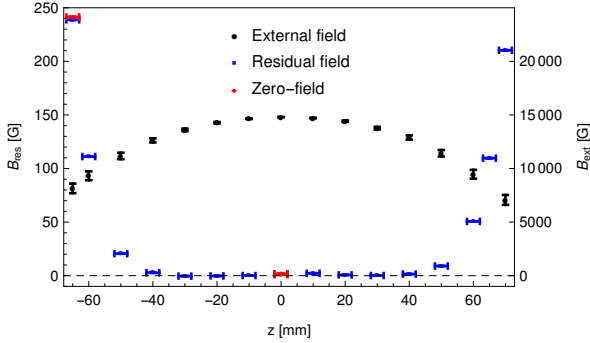


Figure 12: The distribution of B_{res} ($1 \text{ G} = 10^{-4} \text{ T}$) measured along the axis of the Bi-2212 tube (blue squares). The black points show the distribution of B_{ext} ($\sim 1.4 \text{ T}$ at the center). The red diamonds are the values of B_{res} determined from the operation of the Zero-field magnet.

follows:

$$B_z^w(r_x, \Delta_z) = \frac{I^{ext} \mu_0}{4\pi} \int_0^{2\pi} \frac{(R^2 - R r_x \cos \phi)}{(r_x^2 - 2r_x R \cos \phi + R^2 + \Delta_z^2)^{\frac{3}{2}}} d\phi, \quad (5)$$

where Δ_z is the relative distance along the z -axis between the winding center and $P(r_x, r_z)$, R is the radius of the winding, and $\phi \in [0, 2\pi]$ describes the integration over the winding circle. The z -component of the magnetic flux density of one winding is obtained by a summation over the 22 layers of the magnet:

$$B_z^{wn}(r_x, \Delta_z) = \frac{I^{ext} \mu_0}{4\pi} \sum_{n=1}^{n=n_0} \int_0^{2\pi} \frac{(R_n^2 - R_n r_x \cos \phi)}{(r_x^2 - 2r_x R_n \cos \phi + R_n^2 + (\Delta_z - z_n)^2)^{\frac{3}{2}}} d\phi, \quad (6)$$

where the two variables z_n and R_n are functions of the layer number n and describe the position of a single winding in the y - z plane:

$$z_n = ((n-1) \bmod 2) \frac{d_w}{2} \quad (7)$$

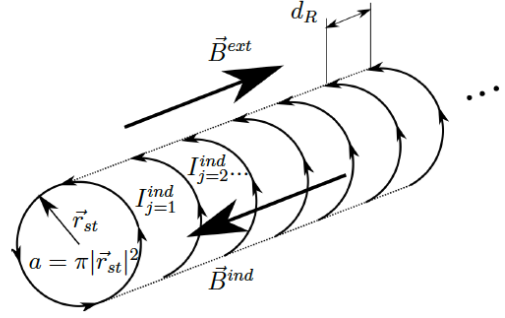


Figure 13: Schematic illustration of the discretization method applied on the shielding tube. The tube is divided in N_{st} equidistant rings at distance d_R . Each of them is carrying a current I_j^{ind} , $j = 1 \dots N_{st}$ induced by the external field \vec{B}^{ext} creating an induced magnetic field \vec{B}^{ind} .

$$R_n = r_{em} + \frac{d_w}{2} + (n-1)\sqrt{3}\frac{d_w}{2}$$

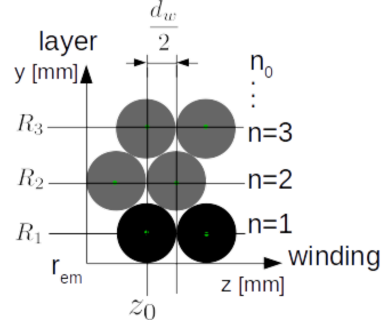


Figure 14: Example of the layout cross section of the external magnet with 2 windings and 3 layers.

3.2. Calculation of the external magnetic flux

The external magnetic flux is calculated based on the arrangement of the magnet and the shielding tube shown in Fig. 15. The external magnetic flux of one winding in a shielding tube ring is

$$F^{wn}(\Delta_z) = 2\pi \int_0^{r_{st}} B_z^{wn}(\rho, \Delta_z) \rho d\rho. \quad (8)$$

The external flux in the shielding tube ring j is calculated by the summation over all windings of the external magnet

$$F_j^{ext} = \sum_{i=1}^{N_{em}} F^{wn}(\Delta_{ij}), \quad (9)$$

where $\Delta_{ij} = |z_i^{em} - z_j^{st}|$ is the distance between the z positions of the i^{th} winding (z_i^{em} , $i = 1 \dots N_{em}$) and the j^{th} ring (z_j^{st} , $j = 1 \dots N_{st}$). Figure 16 shows the external magnetic flux of the external magnet in the shielding tube as a function of z_j^{st} . The value of I^{ext} corresponds to an external magnetic flux density at the center of the tube of 1 T.

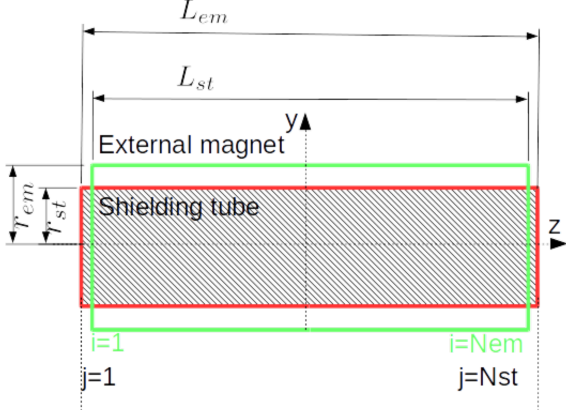


Figure 15: Sketch of the geometry of the external magnet and shielding tube. The shaded area shows the region where the flux of the external magnet is calculated.

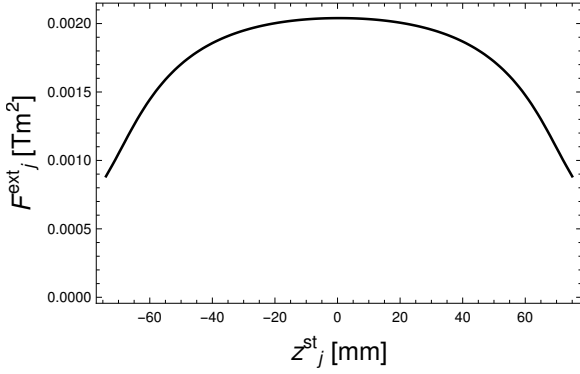


Figure 16: The calculated magnetic flux of the external magnet in the shielding tube.

3.3. Calculation of the induced magnetic flux density

The derivation of the induced current for a system of thin wires can be found in Ref. [14]. The calculations are extended here taking into account the width of the rings in the z -direction. The flux in the ring j of the shielding tube, F_j^{ind} , arising from a ring k , can be expressed as a function the potential vector \vec{A}_k and the cylindrical coordinates shown in Fig. 17, as follows:

$$\vec{A}_k(\phi_j, z_j) = \frac{\mu_0 r_{st}}{4\pi} \int_0^{2\pi} d\phi_k \int_{z_k - \frac{d_R}{2}}^{z_k + \frac{d_R}{2}} dz'_k \frac{\vec{j}_k(\phi_k)}{|\vec{r}_k - \vec{r}_j|},$$

$$\vec{j}_k(\phi_k) = j_k \vec{e}_\phi(\phi_k), j_k = \frac{I_k^{ind}}{d_R}, \quad (10)$$

where \vec{r}_k and \vec{r}_j are the vectors pointing to the k^{th} and j^{th} rings, respectively. The integration is performed over the volume of the k^{th} ring with radius r_{st} and width d_R . The induced magnetic flux F'_j in the j^{th} ring at position z_j generated by the current in the k^{th} ring is

$$F'_j(z'_j) = \int \vec{B}_k \cdot d\vec{a} = r_{st} \int_0^{2\pi} \vec{A}_k \cdot \vec{e}_\phi(\phi_j) d\phi_j, \quad (11)$$

where \vec{B}_k is the magnetic flux density created by the ring k . The flux in a ring F_j^{ind} can be expressed as an average over

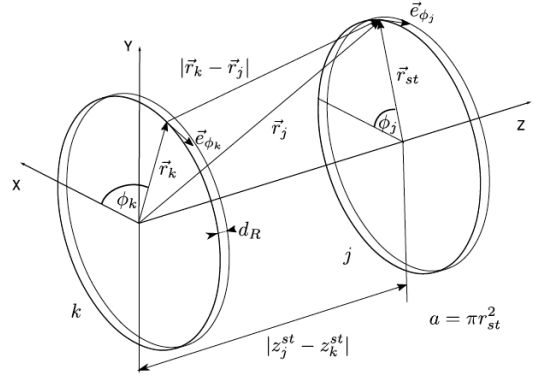


Figure 17: Sketch of two rings with symbols used to calculate the inductance matrix elements.

the flux at a given z , $F'_j(z_j)$, in the interval of the width d_R of the j^{th} ring. Using Eqs. 10 and 11, an inductance matrix element M_{kj} can be defined as follows:

$$F_j^{ind} = M_{kj} I_k^{ind} = -F_j^{ext}, \quad (12)$$

$$M_{kj} = \frac{\mu_0 r_{st}^2}{4\pi d_R^2} \int_{z_j - \frac{d_R}{2}}^{z_j + \frac{d_R}{2}} dz'_j \int_0^{2\pi} d\phi_j$$

$$\int_0^{2\pi} d\phi_k \int_{z_k - \frac{d_R}{2}}^{z_k + \frac{d_R}{2}} dz'_k \frac{\cos(\phi_k - \phi_j)}{|\vec{r}_k - \vec{r}_j|}$$

where a summation over k ($k=1, \dots, N_{st}$) expresses the contributions of all the rings to the flux in the j^{th} ring. The inductance matrix element depends only on the geometry of the rings, in the present case, the radius r_{st} and the ring width d_R . For the diagonal elements of the inductance matrix ($k=j$), a homogenous distribution of the current over the thickness of the ring is assumed [15]:

$$M_{k=j} = \mu_0 r_{st} \left[\ln \frac{8r_{st}}{d_R} - \frac{1}{2} + \frac{d_R^2}{32r_{st}^2} \left(\ln \frac{8r_{st}}{d_R} + \frac{1}{4} \right) \right] \quad (13)$$

The induced current I_j^{ind} is calculated using Eq.13 and the calculated value of F_j^{ext} . The z -component of the induced magnetic flux density created by the current $I_j^{ind} = I^{ind}(z = z(j))$ of the j^{th} ring is

$$B_z^{ring}(r_x = 0, \Delta_z) = \frac{I_j^{ind} \mu_0}{4\pi} \int_0^{2\pi} \frac{R^2}{(R^2 + \Delta_z^2)^{\frac{3}{2}}} d\phi$$

$$= \frac{I_j^{ind} \mu_0}{2} \frac{R^2}{(R^2 + \Delta_z^2)^{\frac{3}{2}}}, \quad (14)$$

where the radius is $R = r_{st}$, and the distance between the rings is $\Delta_z = \Delta_{kj} = |z_k^{st} - z_j^{st}|$. The induced magnetic flux density along the axis of the shielding tube is determined by the summation over all rings

$$B_{r_x=0}^{ind} = \sum_{i=1}^{N_{st}} B_z^{ring}(\Delta_{kj}). \quad (15)$$

The residual magnetic flux density is the superposition of the external and induced magnetic flux densities

$$B^{res} = B^{ext} + B^{ind}. \quad (16)$$

The magnetic flux in the shielding tube of the external magnet at $B_{ext}=1$ T, is calculated and used to calculate the induced current and induced current density by solving Eq. 13. The calculated induced current density for $B_{ext}=1$ T is shown in Fig. 18.

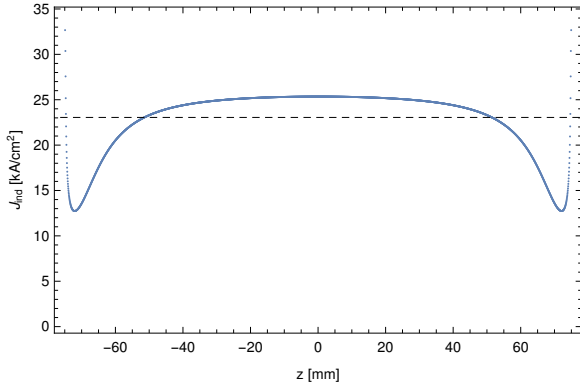


Figure 18: The simulated induced current density along the axis of the shielding tube. The dashed line indicates the average current density.

Figure 19 shows the results of the calculations and the measured values on the external and residual magnetic field densities. The data show a deviation from the simulated curve of the external field. This deviation is assumed to be from the winding errors during the winding of the wire into the layers of a solenoid. The length of the holding structure need to be adjusted to the diameter of the wire. The wire diameter alters in the range between 10 μm and 100 μm due to the uncertainty of the wire coating during the fabrication of the wire and the gluing in the winding procedure. Therefore, the last winding at the end of a layer is not exactly a whole loop. This leads to an imperfection in the profile of the windings resulting in a stronger magnetic field towards the center where the windings are well arranged.

The simulated and measured values of the residual field are consistent within the uncertainties in most of the position points. A small deviation is observed for z -values larger than 40 mm where the measured data points are slightly shifted on the z -axis with respect to the $z = 0$ position. This is assumed to be due to the uncertainty on the manual positioning of the sliding rod and the Hall-probe. This systematic error is not considered in the analysis. The distributions of the residual flux density for different lengths of the shielding tube and the external magnet can be found in Ref. [3]. The numerical stability of the calculation is shown by the robustness of the solution by varying the geometrical parameters and the convergence for refinement of the discretization. It is also shown the homogeneity of the calculated B_{res} in the $x - y$ plane of the shielding tube.

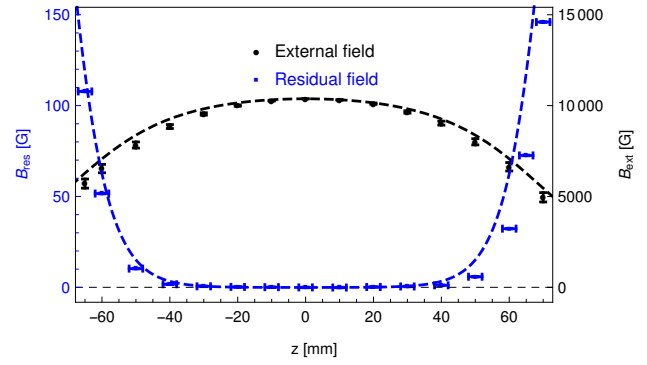


Figure 19: The measured values of B_{res} (blue points) and B_{ext} (black points). The blue and black dashed curves represent the results of the simulations for B_{res} and B_{ext} , respectively (1 G= 10^{-4} T).

4. Summary

The challenging problem of operating a transversely polarized target in a longitudinal magnetic field is addressed. The work is motivated by the possible future upgrade of the $\bar{\text{P}}\text{ANDA}$ spectrometer with the installation of a transversely polarized target. An initial feasibility study for shielding the 2 T longitudinal field created by the $\bar{\text{P}}\text{ANDA}$ solenoid is presented. The shielding performance of a large melt cast Bi-2212 tube in axial magnetic fields is tested at a temperature of 4.2 K. A dedicated apparatus, consisting of the shielding tube, two external magnets, a Hall probe, and a dewar filled with liquid helium is built and used for the measurements. A data acquisition system is developed to control and record the power supply settings and to readout and store the collected data.

It is demonstrated experimentally that a magnetic flux density at the center of the tube of (10140 ± 22) G can be completely shielded, resulting a shielding factor better than $32 \cdot 10^4$. The residual field is monitored for up to 4 days showing a stable shielding operation. In addition, a large volume within the Bi-2212 tube of 150 mm length can be homogeneously shielded. A residual field density less than 1 G is measured over a length of 80 mm at the center. At 1.4 T, B_{res} is measured to be only 1.2 G and increases to 2.7 G after 14 hours of operation. The values of the shielding factor and the induced current density of the shielding tube, determined from the measurements at 1 T and 1.4 T, are summarized in Tab. 8. They show a high shielding performance of the Bi-2212 tube up to 1.4 T.

This feasibility study shows that a Bi-2212 tube, operated at 4.2 K, has the shielding features needed for employing of a transversely polarized target in the presence of intense longitudinal fields. The shielding factor of the Bi-2212 tube at 4.2 K and at an applied external field of 1 T is about two orders of magnitude better than what has been previously achieved at 10 K [11]. High attenuation of the longitudinal magnetic field up to 1.4 T is

External field	1 T	1.4 T
Shielding factor	32×10^4 (95% C.L.)	$(12 \pm 1) \times 10^3$
Induced current density J_{ind} [A/cm ²]	$(23 \pm 2) \times 10^3$	$(33 \pm 3) \times 10^3$
Shielded length [mm] (tube length 150 mm)	80 ± 2	80 ± 2
Residual field after 9 h at 1 T and 14 h at 1.4 T	$(0.0 \pm 2.4) \times 10^{-7}$ T	$(2.70 \pm 0.15) \times 10^{-4}$ T
Residual field in the range of 20 to 80 h	$(0.499 \pm 0.003) \times 10^{-4}$ T	

Table 8: The results of the measurements for the shielding efficiency of the Bi-2212 tube at 4.2 K for applied axial fields of 1 T and 1.4 T. The tube length is 150 mm and has a wall thickness of 3.5 mm.

proven. Based on this study, a dedicated prototype that fulfills the geometrical and the performance requirements of the \bar{P} ANDA experiment can be designed. The numerical calculations that are developed here and validated by the experimental tests can be used for this purpose.

Acknowledgments

We acknowledge the support from the A2 Collaboration and the mechanical and the electronics workshops at the Institute for the Nuclear Physics (Mainz, Germany) in the preparation of the apparatus and the realization of the measurements. B. F. acknowledges useful and inspiring discussions with Christian Kremers from Dassault Systèmes and Steffen Elschner from the University of Applied Science Mannheim. We thank Florian Feldbauer, Cristina Morales and Patricia Aguar Bartolome (Helmholtz-Institut Mainz) and Oleksandr Kostikov (Institute of Nuclear Physics, Mainz) for their help in this work and/or for taking shifts during the measurements.

References

- [1] W. Erni, et al., *Physics Performance Report for PANDA: Strong Interaction Studies with Antiprotons* (2009). [arXiv:0903.3905](#).
- [2] G. Barucca, et al., *Eur. Phys. J. A* 57 (6) (2021) 184. [doi:10.1140/epja/s10050-021-00475-y](#).
- [3] B. Fröhlich, *Investigation on intense magnetic flux shielding with a high temperature superconducting tube for a transverse polarized target at the \bar{P} ANDA experiment*, Ph.D. thesis, Mainz U. (2017). [doi:10.25358/openscience-1178](#).
- [4] S. Denis, et al., *Superconductor Science and Technology* 20 (5) (2007) 418–427. [doi:10.1088/0953-2048/20/5/002](#).
- [5] J.-F. Fagnard, et al., *Superconductor Science and Technology* 22 (10) (2009) 105002. [doi:10.1088/0953-2048/22/10/105002](#).
- [6] M. Miller, et al., *Cryogenics* 33 (2) (1993) 180–183. [doi:https://doi.org/10.1016/0011-2275\(93\)90133-9](#).
- [7] V. Plecháček, E. Pollert, J. Hejtmánek, *Materials Chemistry and Physics* 43 (2) (1996) 95–98. [doi:https://doi.org/10.1016/0254-0584\(95\)01627-7](#).
- [8] T. Cavallin, R. Quarantiello, A. Matrone, G. Giunchi, *Journal of Physics: Conference Series* 43 (2006) 1015–1018. [doi:10.1088/1742-6596/43/1/248](#).
- [9] P. Fournier, M. Aubin, *Phys. Rev. B* 49 (1994) 15976–15983. [doi:10.1103/PhysRevB.49.15976](#).
- [10] M. Statera, Others, *Nuclear Instruments and Methods in Physics Research. Section A, Accelerators, Spectrometers, Detectors and Associated Equipment* 882. [doi:10.1016/j.nima.2017.10.051](#).
- [11] J.-F. Fagnard, et al., *Superconductor Science and Technology* 23 (9) (2010) 095012. [doi:10.1088/0953-2048/23/9/095012](#).

- [12] J. Bock, S. Elschner, P. Herrmann, *IEEE Transactions on Applied Superconductivity* 5 (2) (1995) 1409–1412. [doi:10.1109/77.402828](#).
- [13] Z. Feng, *IEEE Transactions on Magnetics* 21 (2) (1985) 993–996. [doi:10.1109/TMAG.1985.1063600](#).
- [14] J. D. Jackson, *Classical Electrodynamics, sect. 5.17, third edition* (1999).
- [15] E. B. Rosa, *Bulletin of the Bureau of Standards, Vol. 4., No. 3., p. 372*.